RM E55D04

NACA

RESEARCH MEMORANDUM

STATIC INVESTIGATION OF SEVERAL JET DEFLECTORS FOR LONGITUDINAL CONTROL OF AN AIRCRAFT

By Alfred S. Valerino

Lewis Flight Propulsion Laboratory
Cleveland, Ohio

NATIONAL ADVISORY COMMITTEE
FOR AERONAUTICS

WASHINGTON

June 7, 1955
Declassified April 8, 1957.

NATIONAL ADVISORY COMMITTEE FOR AERONAUTICS

RESEARCH MEMORANDUM

STATIC INVESTIGATION OF SEVERAL JET DEFLECTORS FOR LONGITUDINAL CONTROL OF AN AIRCRAFT

By Alfred S. Valerino

SUMMARY

The lift and drag characteristics of five jet deflectors of semicircular cross section, mounted at the exit of a shrouded iris-flap, afterburner-off ejector, were investigated in quiescent air over a range of deflector angles, primary-nozzle pressure ratios, and secondary weight flows. The deflectors were alined with either the trailing edge of the afterbody shroud or with the trailing edge of the shrouded iris flap for afterburner-off operation. Data were also obtained for two deflectors mounted at the exit of an ejector without iris flaps to simulate afterburner-on operation.

Results of the investigation indicated that deflector length, wetted area, and radial location with respect to jet boundary had marked and interrelated effects on the deflector lift and drag forces. When the deflector was alined with the trailing edge of the afterbody shroud (deflector removed from jet boundary), the lowest lifts per unit deflector area were obtained with the deflector of the shortest length. When the deflector was alined with the trailing edge of the shrouded iris flap (deflector near jet boundary), the highest lifts per unit area were obtained with the deflector of the shortest length.

INTRODUCTION

One of the problems encountered in some present-day aircraft is that of uncontrolled pitch-up during landing or take-off. Several methods for generating aircraft control forces at low speeds have been investigated. These include the use of movable vanes or plates located externally in the exhaust jet (refs. 1 to 4), a deflection vane inside the primary nozzle (ref. 5), and a swiveling nozzle (ref. 5). The investigation reported herein employed radially curved jet deflectors attached to the afterbody shrouds of several ejector nozzles.

Experimental data were obtained in quiescent air with primary nozzles simulating either the afterburner-on or afterburner-off operation. The investigation was conducted through a range of primary-nozzle pressure ratios of 2 to 9 with variable secondary flow. The jet deflectors were rotated through a range of angles from $-4\frac{1}{2}^{\circ}$ to 40°. Temperature of the exhaust jet was maintained at approximately 710° R.

APPARATUS AND PROCEDURE

The model was installed in the lower balance chamber of the Lewis 8- by 6-foot supersonic wind tunnel as shown in figure 1. Preheated high-pressure air was supplied to the model through hollow support struts. A detailed discussion of the air-supply system is presented in reference 6. Primary-nozzle pressure ratio was set by simultaneously regulating the total pressure of the preheated air supplied to the model and the ambient discharge pressure.

A sketch of the model is presented in figure 2. The three ejector configurations shown in figure 3 were utilized. Two configurations simulated afterburner-off operation with reduced nozzle throat and exit areas, while the third simulated afterburner-on operation. The deflectors A, B, C, D, and E shown in figure 4 were used with these ejector configurations. All the deflectors had the same semicircular cross section (radius, 2.44 in.). Deflectors B and C were obtained by cutting deflector A as indicated in figure 4(a). Deflectors D and E were obtained by cutting 0.3 inch from the leading edge of deflectors A and C, respectively, and are shown in figure 4(b).

With the afterburner-off configurations, the deflectors were located in the following two positions with respect to the model horizontal centerline: (1) deflectors A, B, and C were mounted to aline with the afterbody shroud trailing edge as shown in figure 3(a), hereinafter referred to as configuration I; (2) deflectors D and E were mounted to aline with the iris-flap trailing edge as shown in figure 3(b), hereinafter referred to as configuration II. With the afterburner-on configuration (configuration III), deflectors D and E were mounted to aline with the trailing edge of the afterbody shroud as shown in figure 3(c) (note absence of iris flaps). Photographs of deflector (D) mounted on configurations II and III are presented in figure 5.

Lift and axial forces were measured by two single-component strain-gage units. The lift strain gage was external to the model but was linked to the afterbody as shown in figures 1 and 2. The axial-component strain gage was mounted internally.

DISCUSSION OF RESULTS

The experimental lift and drag forces are presented as fractions of a reference force that is equal to the product of ambient pressure and the deflector projected plan-form area at zero deflection. The drag presented herein is defined as the loss in force due to the presence of the deflector. Ejector gross forces for configurations without deflectors are presented so that an estimate of the drag penalties, in terms of ejector gross force, can be evaluated.

Afterburner-off configurations. - The effects of deflector angle β on the performance of configurations I and II at primary-nozzle pressure ratios P_p/p_0 of 2, 3, and 4 are presented in figures 6, 7, and 8, respectively. The lift parameter increased with increasing primary-nozzle pressure ratio and deflector angle (figs. 6 to 8). Since the flow was overexpanded at the test values of primary-nozzle pressure ratios, negative lifts resulted at the lower deflector angles. At a given deflector angle, higher lifts resulted with deflectors D and E of configuration II than with deflectors A, B, and C of configuration I because the deflectors of configuration II were closer to the jet boundary.

With configuration I, throughout most of the range of variables investigated, the lift parameter of deflector B was comparable to that of deflector A at the same conditions. Thus, removing a small portion of the sides of the deflector without decreasing its length was not detrimental to the lift parameter. However, cutting deflector A to form deflector C reduced both the deflector length and effective wetted area, resulting in a decrease in lift parameter over most of the range of deflector angles. When the deflectors were moved closer to the jet boundary (configuration II), a large decrease in deflector length and wetted area did not penalize the lift parameter. The largest lift parameters were obtained with deflector E rather than with deflector D, which had the larger projected area and the larger net lift.

The drag parameter, like the lift parameter, also increased with increasing primary-nozzle pressure ratio and deflector angle. Generally, the drag increased sharply at deflector angles slightly higher than the angle required for positive lift. Since the deflectors of configuration I were not as close to the jet as those of configuration II, lower drag parameters were obtained with deflectors A, B, and C at given deflector angles. Deflector E, which had the highest lift parameters, generally had the highest drag parameters throughout the deflector-angle range.

Afterburner-on configuration. - Lift and drag parameters of deflector D with configuration III are presented for primary-nozzle pressure ratios of 3.8, 7, and 9 in figure 9.

At a primary-nozzle pressure ratio of 3.8 where the flow is overexpanded, negative lifts were obtained. A comparison of the lift parameters at a primary-nozzle pressure ratio of 3.8 with those obtained with configuration II deflector D at a primary-nozzle pressure ratio of 4 (fig. 8) indicates that slightly higher lifts were obtained with configuration III.

Increasing the primary-nozzle pressure ratio again generally resulted in an increase in lift and drag parameters. The value of secondary weight-flow ratio at which the highest lift and lowest drag parameters were obtained varied with the primary-nozzle pressure ratio.

A comparison of the experimental lift and drag parameters for configuration III at zero secondary weight flow with those computed from a simplified theory is presented in figure 10. The theory is applied only at angles below the shock detachment angle of 17°. Neglected in the theory are deflector tip and chord effects. A friction drag increment of 0.2, estimated from the experimental data at zero deflection angle, was added to the theoretical drag. The symbols used and an evaluation of the theoretical lift and drag parameters are given in appendixes A and B, respectively. The dashed portion of the curves presented in figure 10 represent a faired interpolation from the detachment angle of 17° to the maximum drag angle of 90°. The comparison shows that the simplified relations overestimate the lift parameter. However, better agreement with experiment is obtained on a drag and lift-drag-ratio basis. The theory appears to reasonably predict the trend of the variation of the lift-drag ratio with deflector angle.

SUMMARY OF RESULTS

From a quiescent-air investigation of the lift and drag forces of five radially curved jet deflectors (mounted at the exit of a shrouded iris-flap ejector) the following results were obtained:

1. The deflector lift and drag forces were affected by the deflector length, wetted area, and radial location with respect to the ejector jet in a complex relation. For example, when the deflector was alined with the trailing edge of the ejector afterbody shroud (deflector removed from jet boundary), the lowest lifts per unit deflector area were obtained with the deflector of the shortest length. However, when the deflector was alined with the trailing edge of the shrouded iris flap (deflector near jet boundary), the highest lifts per unit deflector area were obtained with the deflector of the shortest length.

Lewis Flight Propulsion Laboratory
National Advisory Committee for Aeronautics
Cleveland, Ohio, April 5, 1955

APPENDIX A

SYMBOLS

The following symbols are used in this report:

A	area of deflector projected to a plane through horizontal centerline of deflector, sq ft.
c	deflector chord length
D	drag, loss in net propulsive force due to deflector
D/p_0A	drag parameter
F_e	gross force of ejector without deflector
F_e/p_0A	ejector gross-force parameter
L	lift due to deflector
L/p_0A	lift parameter
L/D	lift-drag ratio
N	normal force
P	total pressure
P_p/p_0	primary-nozzle total pressure ratio
p	static pressure
r	deflector radius
T	total temperature, $^{\circ}R$
W	weight flow, lb/sec
$\frac{W_s}{W_p}\sqrt{\frac{T_s}{T_p}}$	corrected weight-flow ratio
β	deflector angle, deg
θ	radial position along curved deflector

Subscripts:

e	ejector
p	primary nozzle
s	secondary passage
0	free stream or ambient
1	nozzle exit station
2	ejector exit station
3	station at lower surface of deflector

APPENDIX B

EVALUATION OF THEORETICAL LIFT AND DRAG PARAMETERS

Evaluation of lift and drag forces for configuration III as determined by the following analysis is similar to that reported in reference 7 except that shock relations replace the linearized theory. The following sketch is included to aid in the evaluation:

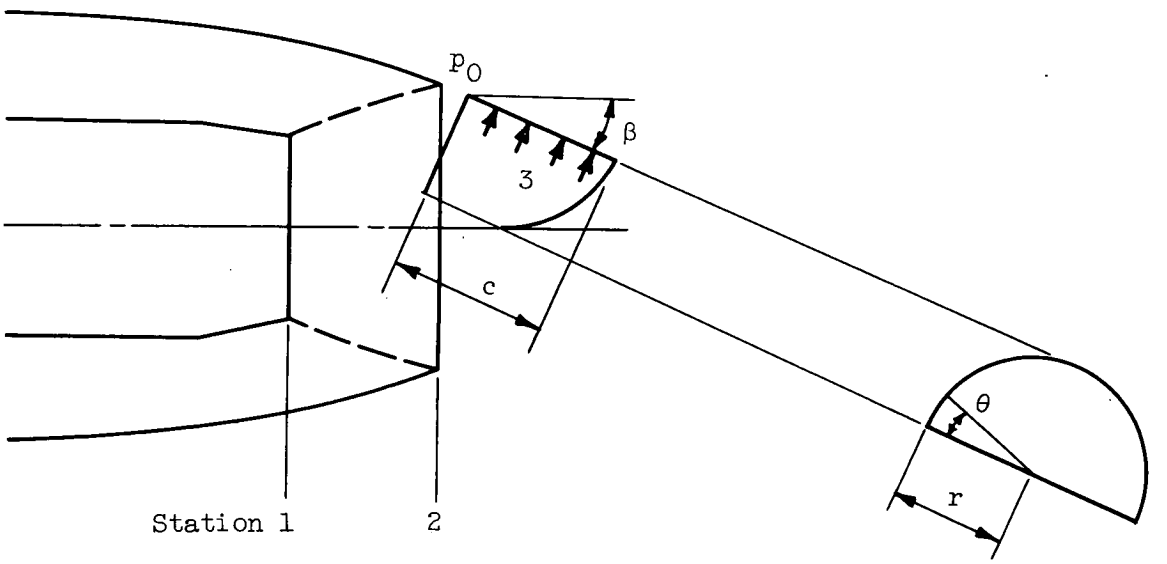

The following assumptions were made for the analysis:

(1) The primary-nozzle jet is fully expanded from station 1 (nozzle exit) to fill the passage at station 2 (ejector exit) with no loss in total pressure.

(2) There is no chordwise pressure gradient on the deflector.

(3) Friction drag on the deflector is given by $D/p_0A = 0.2$.

(4) There is no gap effect.

The lift force of the deflector is

$$L = N \cos \beta \tag{B1}$$

where

$$N = \int_0^{\pi} (p_3 - p_0)\, cr \sin \theta \, d\theta \tag{B2}$$

From equations (B1) and (B2),

$$L = \cos \beta \int_0^{\pi} (p_3 - p_0)\, cr \sin \theta \, d\theta \tag{B3}$$

The lift parameter $\frac{L}{p_0 A}$ is equal to

$$\left.\begin{aligned} &\frac{\cos \beta \, cr}{2\, cr} \int_0^{\pi} \left(\frac{p_3 - p_0}{p_0}\right) \sin \theta \, d\theta \\ &= \frac{\cos \beta}{2} \int_0^{\pi} \left(\frac{p_3 - p_2}{p_0} + \frac{p_2 - p_0}{p_0}\right) \sin \theta \, d\theta \end{aligned}\right\} \tag{B4}$$

$$= \frac{\cos \beta}{2} \left(\frac{p_2}{p_0}\right) \int_0^{\pi} \left(\frac{p_3}{p_2} - 1\right) \sin \theta \, d\theta + \frac{\cos \beta}{2} \int_0^{\pi} \left(\frac{p_2}{p_0} - 1\right) \sin \theta \, d\theta \tag{B5}$$

therefore

$$\frac{L}{p_0 A} = \frac{\cos \beta}{2} \left(\frac{p_2}{p_0}\right) \int_0^{\pi} \left(\frac{p_3}{p_2} - 1\right) \sin \theta \, d\theta + \cos \beta \left(\frac{p_2}{p_0} - 1\right) \tag{B6}$$

where $p_2/p_0 = (P_1/p_0)(p_2/P_1)$, and p_3/p_2 is obtained from two-dimensional relations where the local deflection angle is taken equal to $\beta \sin \theta$. The first part of equation (B6) is obtained by graphical integration.

The drag parameter is

$$\frac{D}{p_0 A} = \frac{N \sin \beta}{p_0 A} + 0.2 = \frac{L \tan \beta}{p_0 A} + 0.2 \tag{B7}$$

where 0.2 is assumed as the friction drag parameter.

Equations (B6) and (B7) were used to evaluate the lift and drag parameters to $\beta = 17^{\circ}$. At angles greater than 17°, the two-dimensional shock detaches. At $\beta = 90^{\circ}$, the lift force will be zero. The drag force at $\beta = 90^{\circ}$ was computed assuming p_3 equal to normal shock

value. For deflector angles between 17° and 90°, the drag-parameter curve was faired to fit the computed end points. From the drag curve and equation (B7), the lift parameters for angles between 17° and 90° were obtained.

REFERENCES

1. Rose, C. H., and Immenschuh, W. T.: Report on Engineering Study and Investigation of the Problems of Jet Thrust System as Related to Control of an Airplane, Pts. I and II. Final Reps. Nos. 3817-6, Ryan Aero. Co., San Diego (Calif.), Apr. 28, 1948.

2. Bond, Aleck C.: Experimental Investigation of a Flat-Plate Paddle Jet Vane Operating on a Rocket Jet. NACA RM L50I20, 1950.

3. Wineman, Andrew R.: Preliminary Investigation of a Fin-Actuated Jet-Vane Control System for Stabilization of Rocket-Powered Models. NACA RM L50K17, 1951.

4. Anon.: Jet-Vane Controlled Bomber Defense Missile. Rep. No. BE-753-S4, Quart. Prog. Rep. No. 2, Cornell Aero. Lab., Inc., July-Sept. 1951. (Contract AF 33(038)-22346, MX-1601.)

5. Englert, Gerald W., and Leissler, L. Abbott: Preliminary Wind-Tunnel Investigation of Two Types of Jet-Exit Configurations for Control of Aircraft. NACA RM E54E27, 1954.

6. Stitt, Leonard E., and Valerino, Alfred S.: Effect of Free-Stream Mach Number on Gross-Force and Pumping Characteristics of Several Ejectors. NACA RM E54K23a, 1955.

7. Mirels, Harold: Theoretical Wave Drag and Lift of Thin Supersonic Ring Airfoils. NACA TN 1678, 1948.

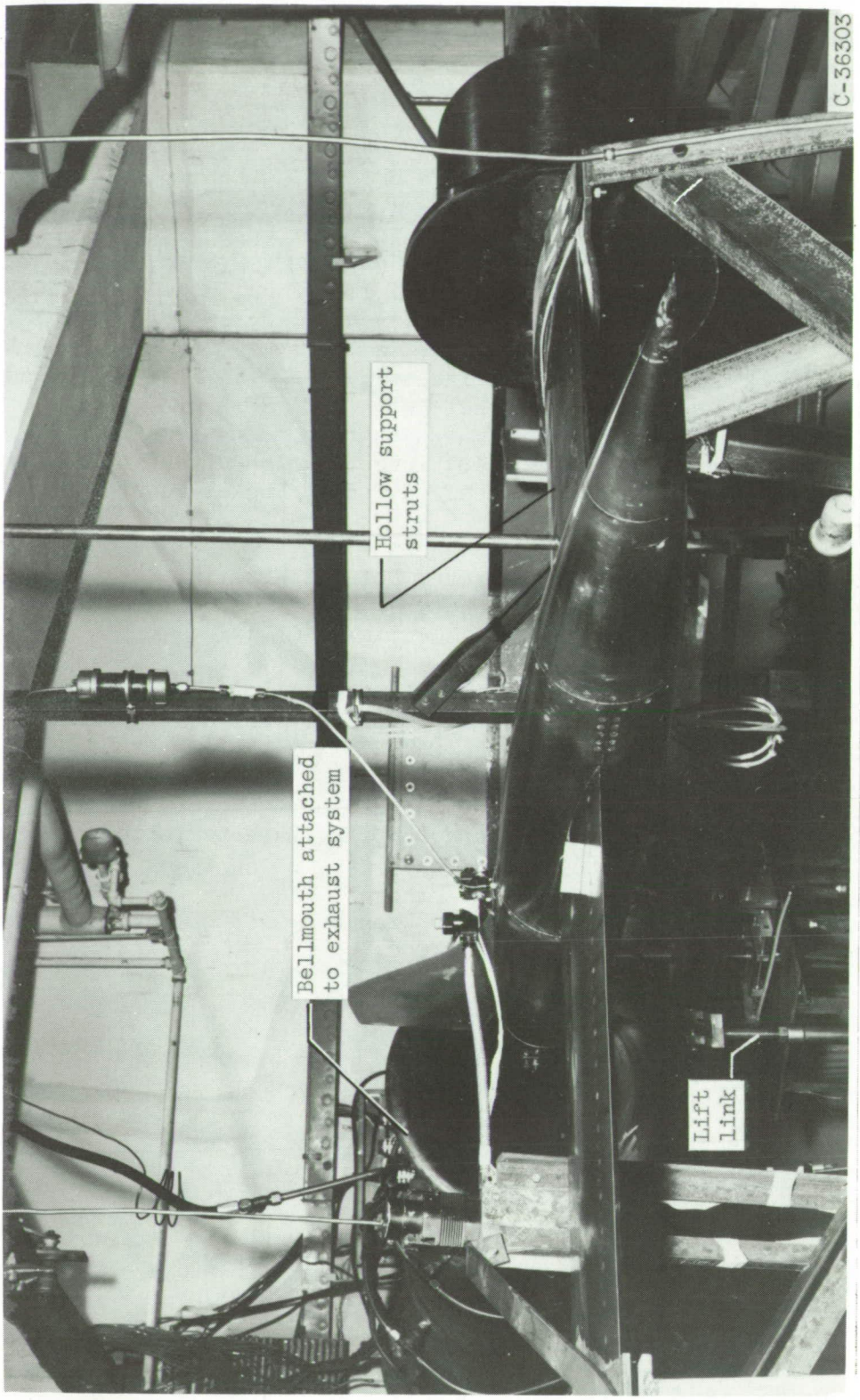

Figure 1. - Static test rig.

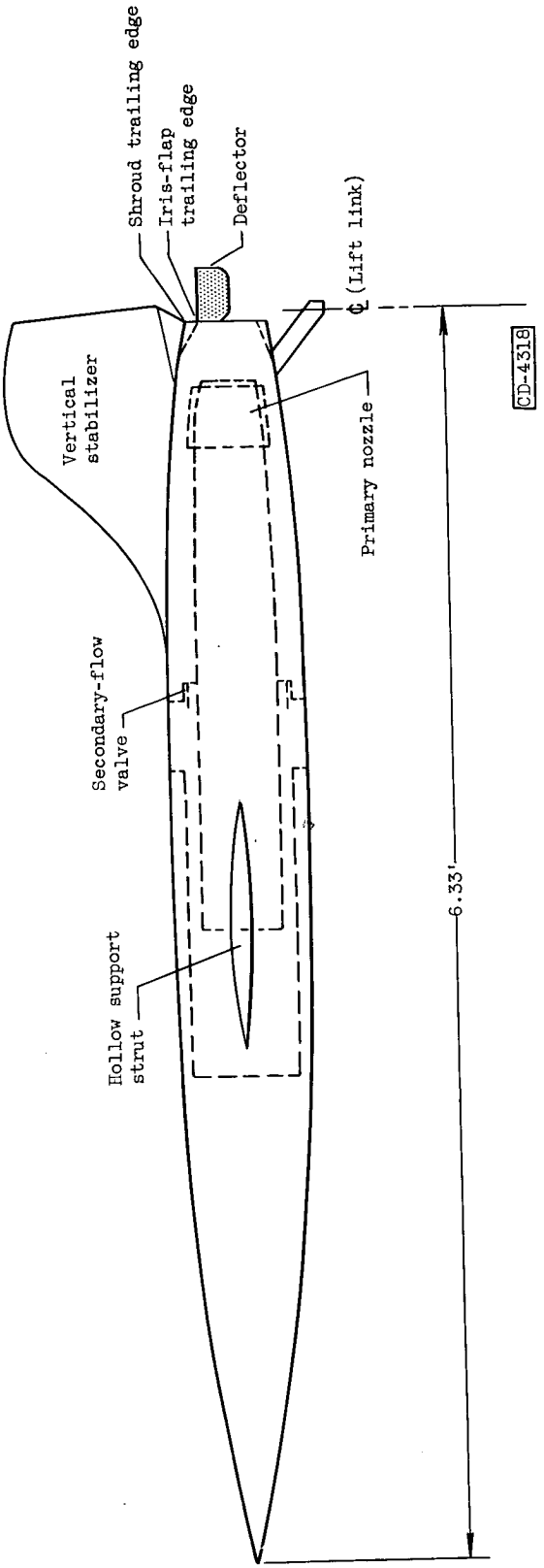

Figure 2. - Model installation.

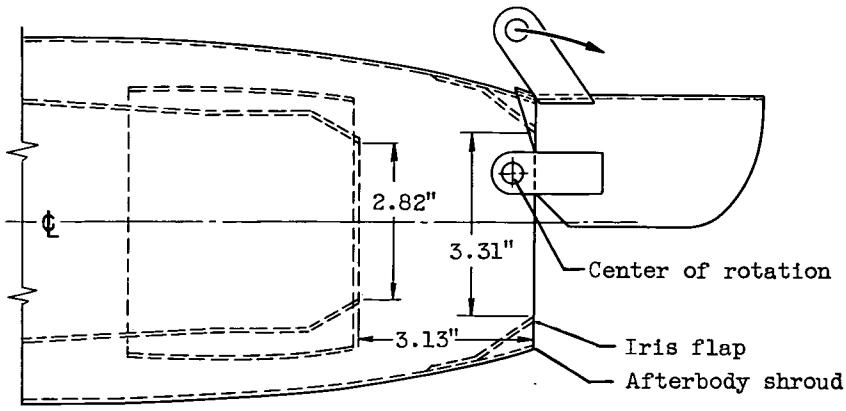

(a) Configuration I. Deflector A at trailing edge of afterbody shroud; afterburner-off operation; diameter ratio, 1.17; spacing ratio, 1.10.

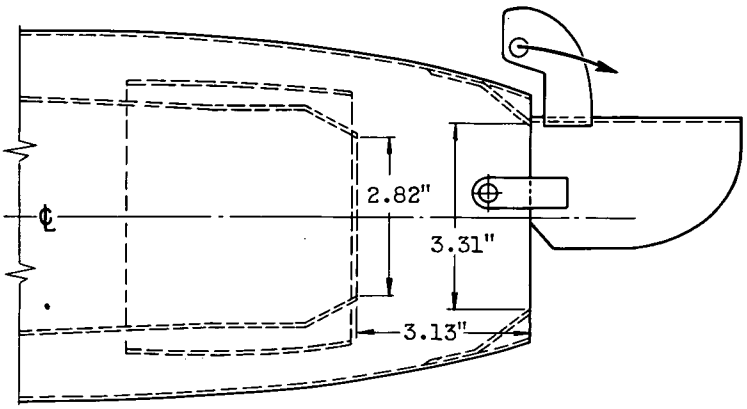

(b) Configuration II. Deflector D at trailing edge of iris flap; afterburner-off operation; ejector diameter ratio, 1.17; spacing ratio, 1.10.

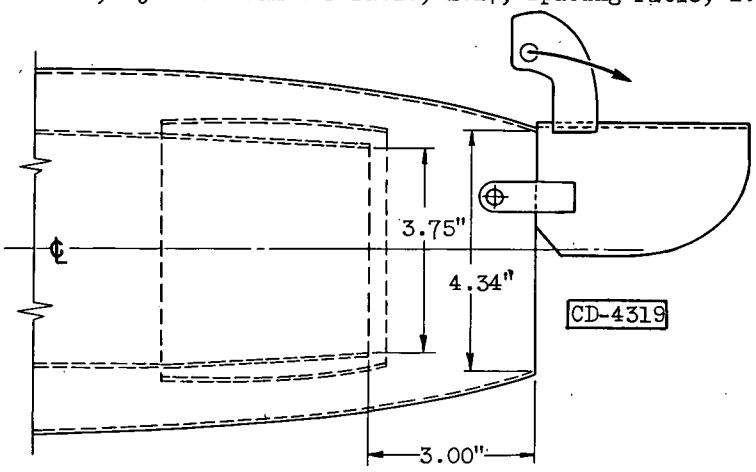

(c) Configuration III. Deflector D at trailing edge of afterbody shroud; afterburner-on operation; ejector diameter ratio, 1.16; spacing ratio, 0.80.

Figure 3. - Sketch of configurations showing position of deflectors with respect to afterbody shroud and iris flap.

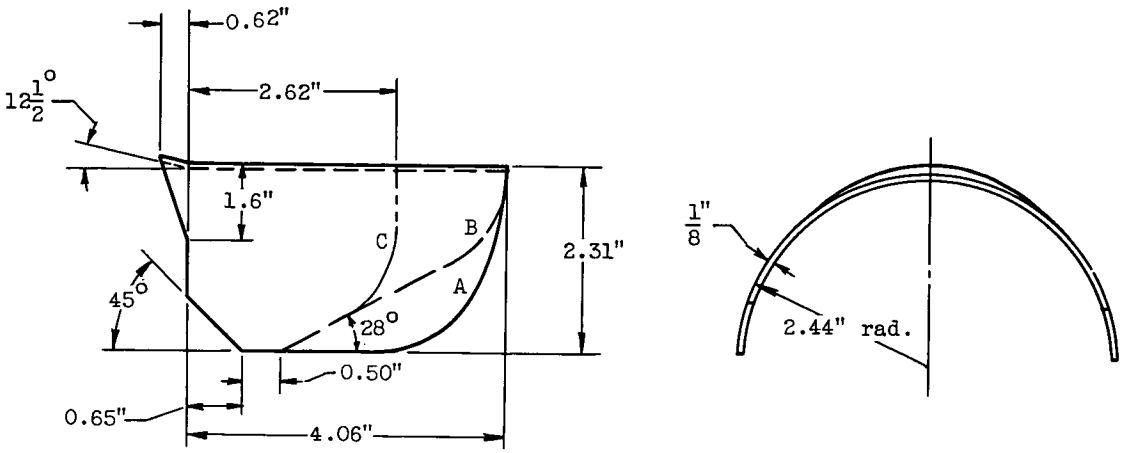

(a) Deflectors used with configuration I.

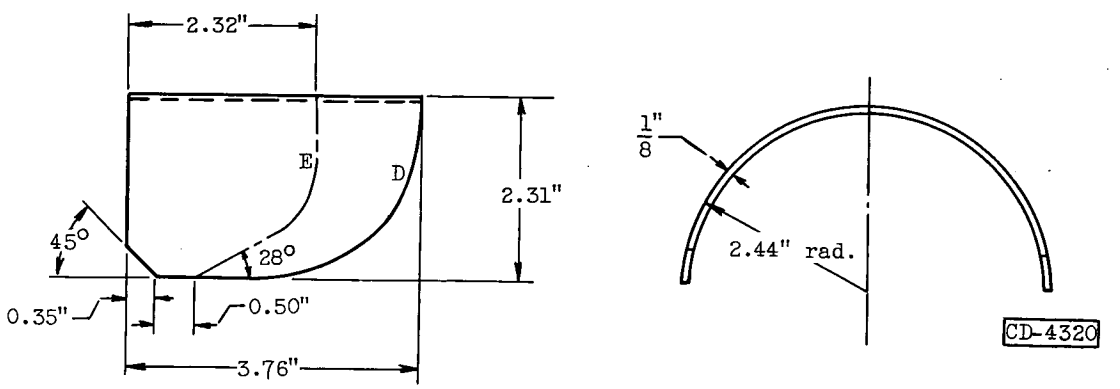

(b) Deflectors used with configurations II and III.

Figure 4. - Superimposed sketches of deflectors showing modifications.

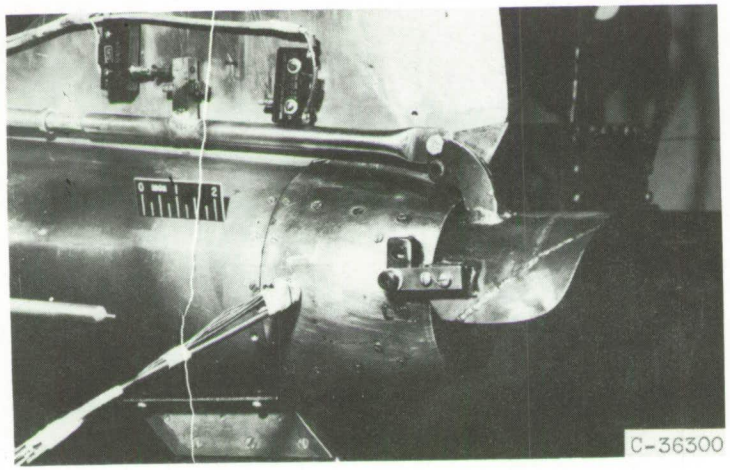

(a) Configuration II; deflector D; angle, 0°.

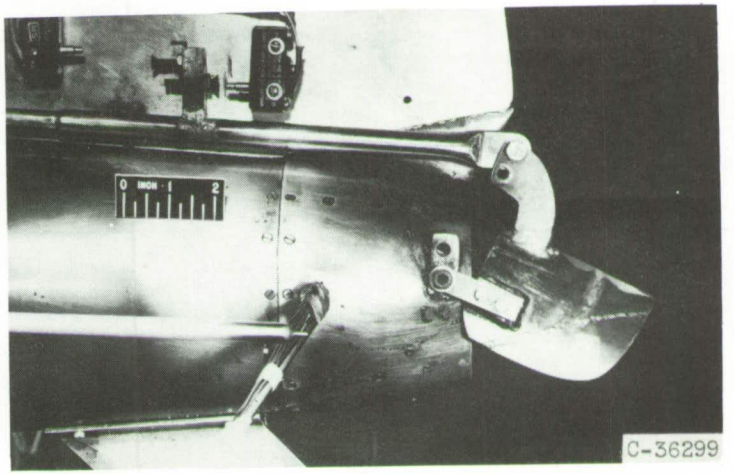

(b) Configuration II; deflector D; angle, 20°.

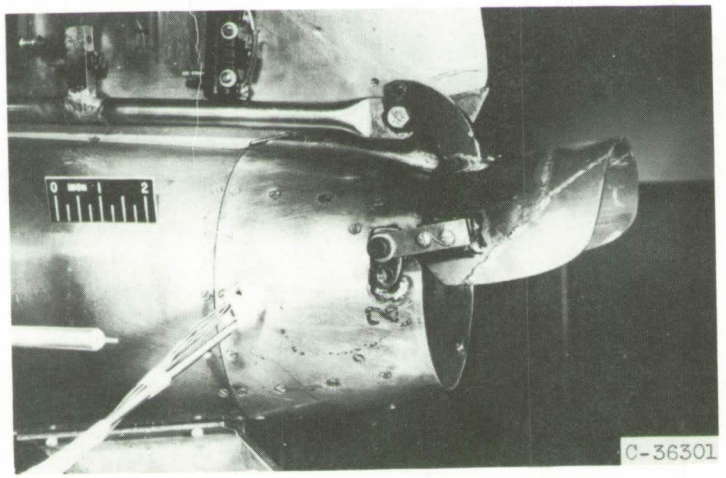

(c) Configuration III; deflector D; angle, $-3\frac{1}{2}^{\circ}$.

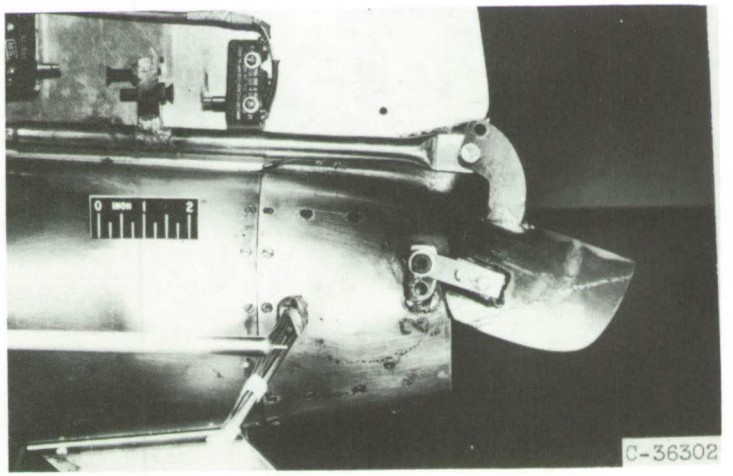

(d) Configuration III; deflector D; angle, 15°.

Figure 5. - Deflector D mounted on configurations II and III at various angles.

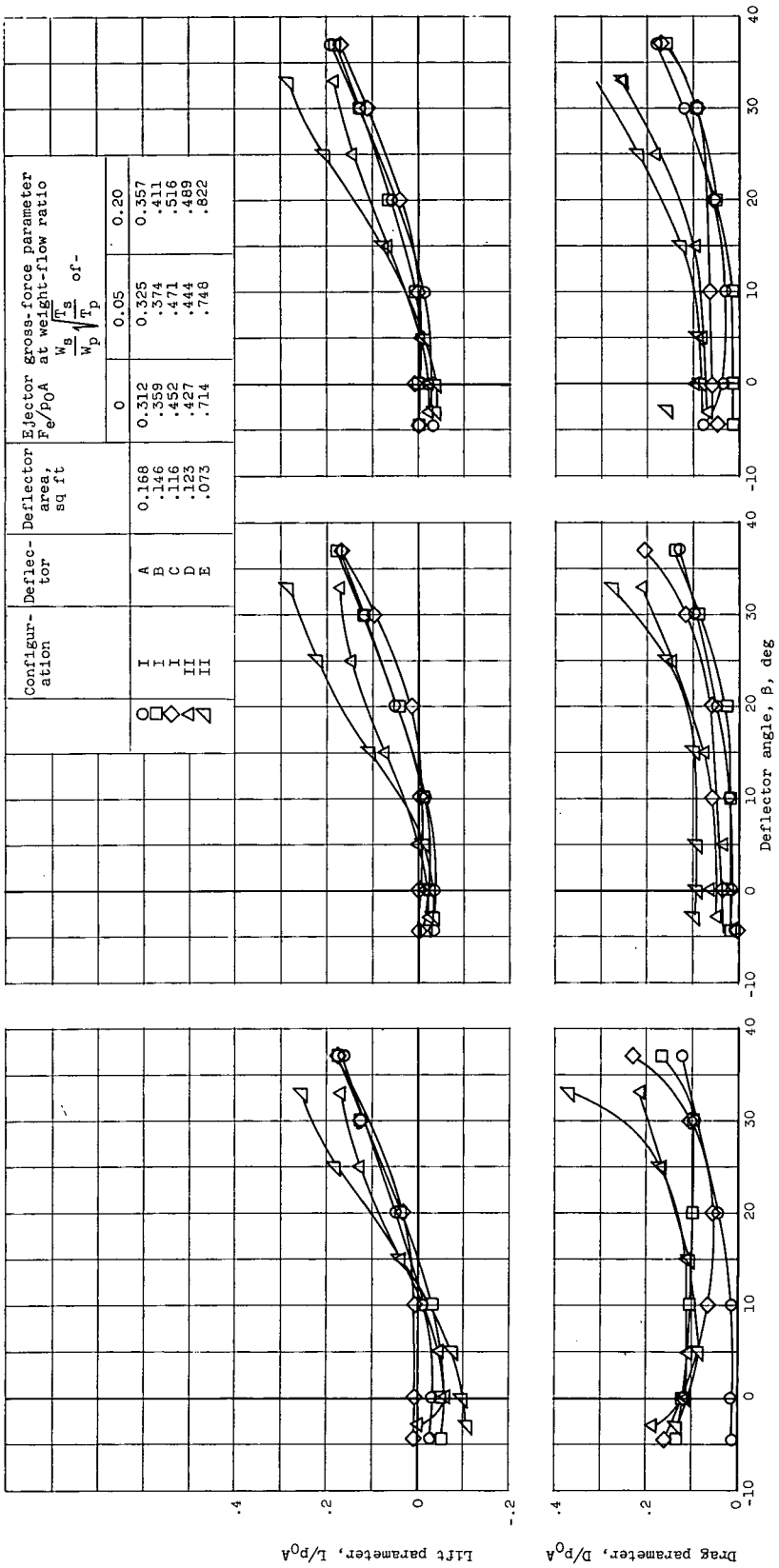

(a) Secondary-to-primary weight-flow ratio, zero.

(b) Secondary-to-primary weight-flow ratio, 0.05.

(c) Secondary-to-primary weight-flow ratio, 0.20.

Figure 6. - Effect of deflector angle on lift and drag parameters of configurations I and II. Primary-nozzle pressure ratio, 2.

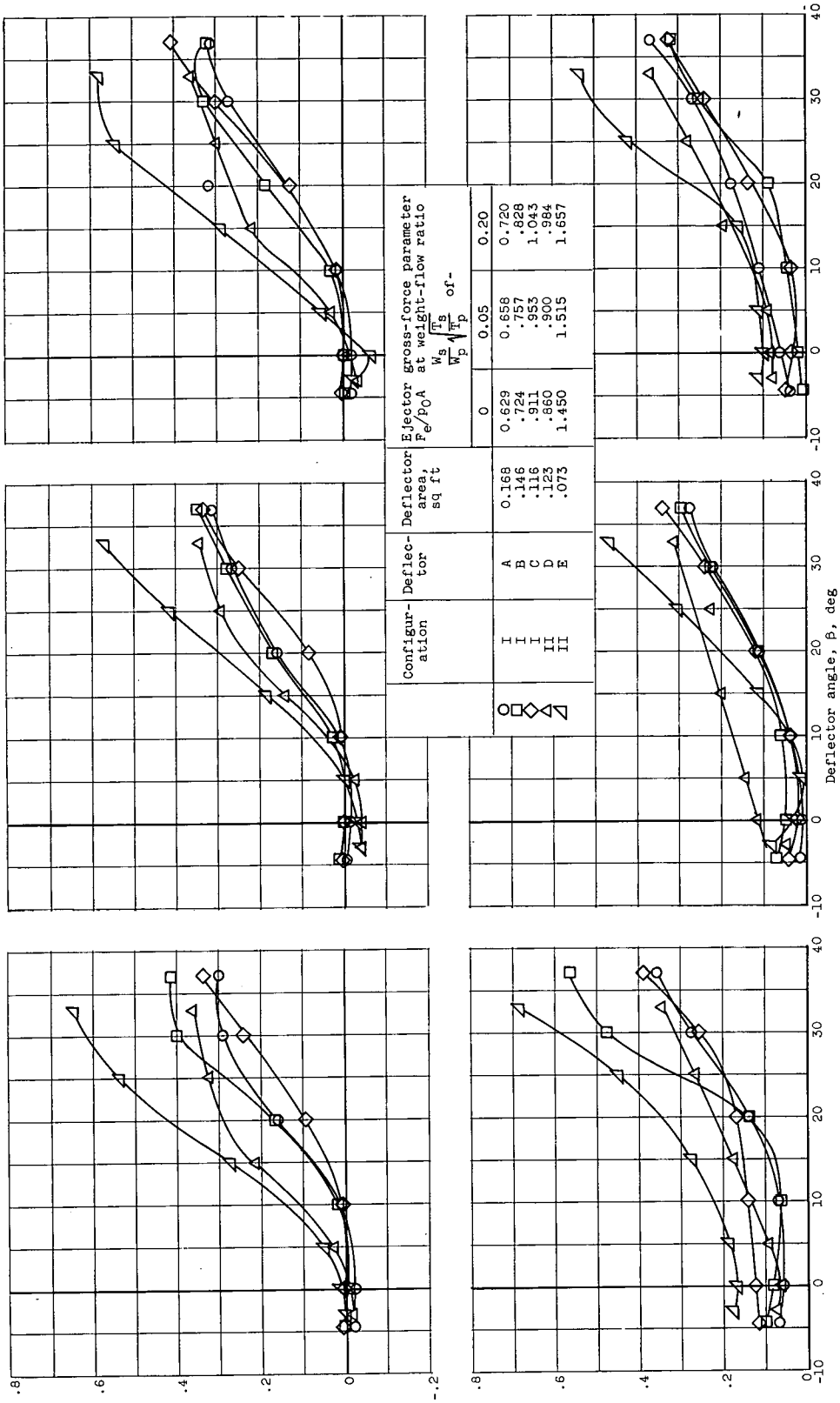

(a) Secondary-to-primary weight-flow ratio, zero. (b) Secondary-to-primary weight-flow ratio, 0.05. (c) Secondary-to-primary weight-flow ratio, 0.20.

Figure 7. - Effect of deflector angle on lift and drag parameters of configurations I and II. Primary-nozzle pressure ratio, 3.

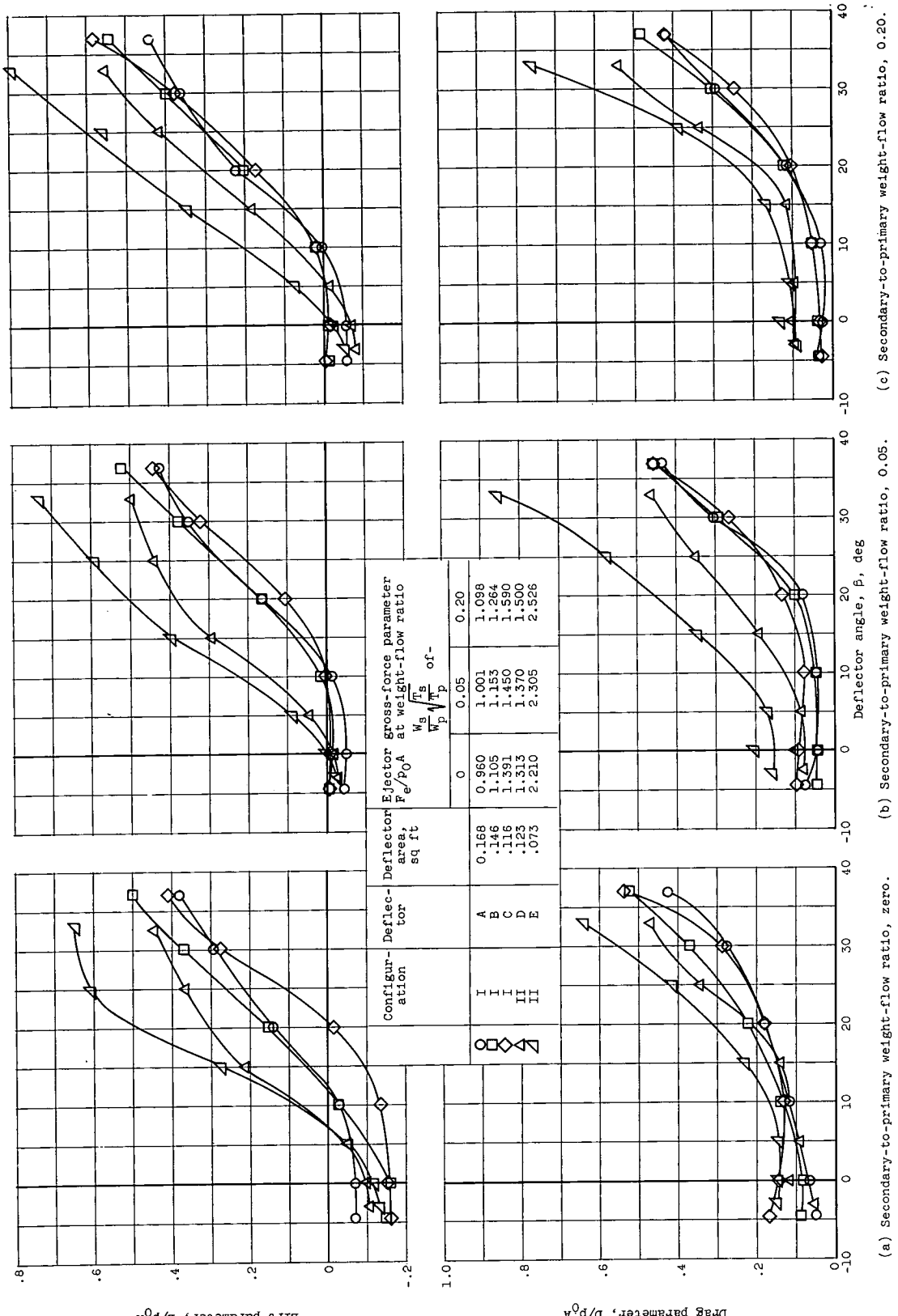

(a) Secondary-to-primary weight-flow ratio, zero.

(b) Secondary-to-primary weight-flow ratio, 0.05.

(c) Secondary-to-primary weight-flow ratio, 0.20.

Figure 8. - Effect of deflector angle on lift and drag parameters of configurations I and II. Primary-nozzle pressure ratio, 4.

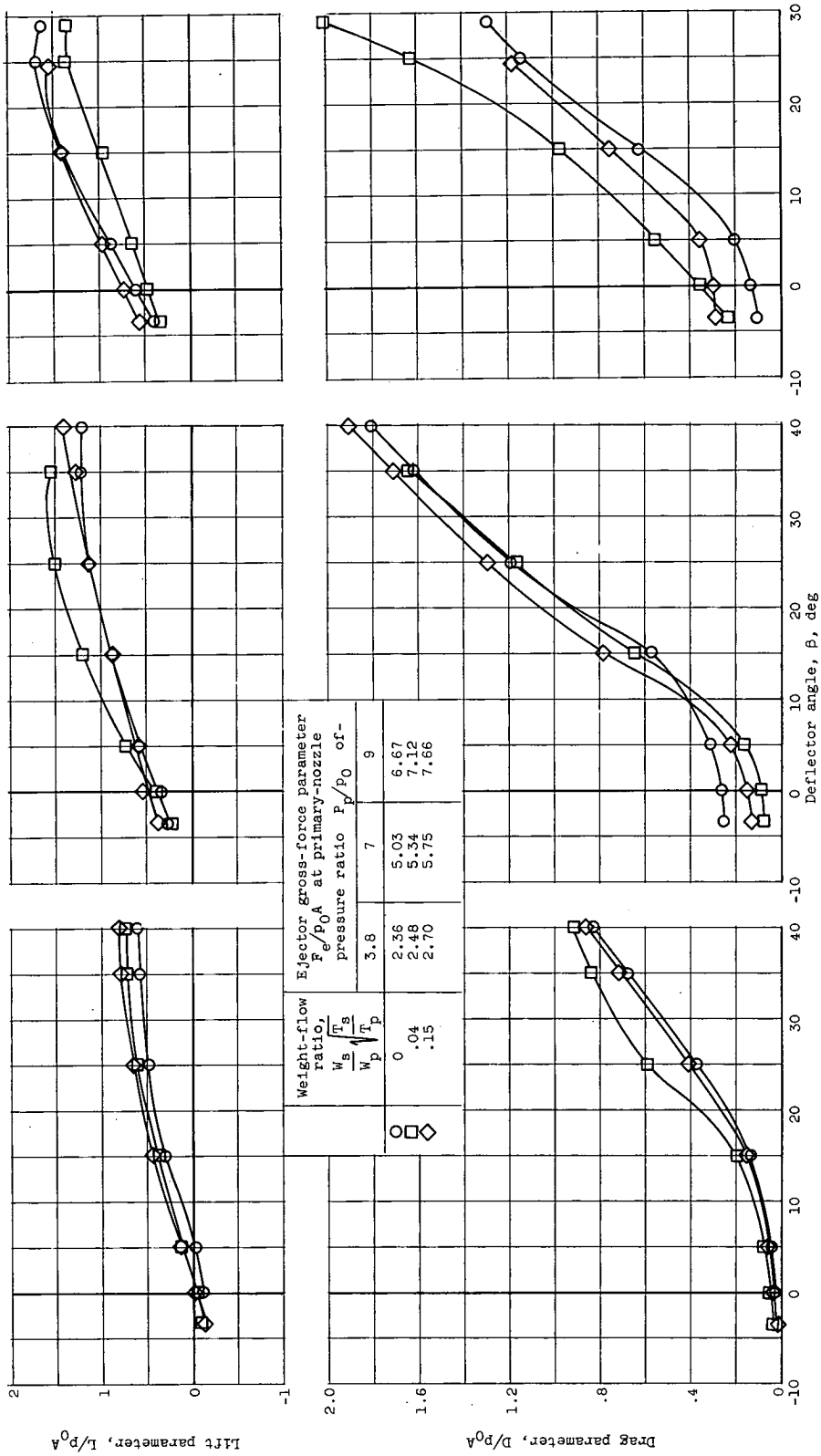

(a) Primary-nozzle pressure ratio, 3.8. (b) Primary-nozzle pressure ratio, 7. (c) Primary-nozzle pressure ratio, 9.

Figure 9. - Effect of deflector angle on lift and drag parameters of configuration III. Deflector D with area of 0.123 square feet.

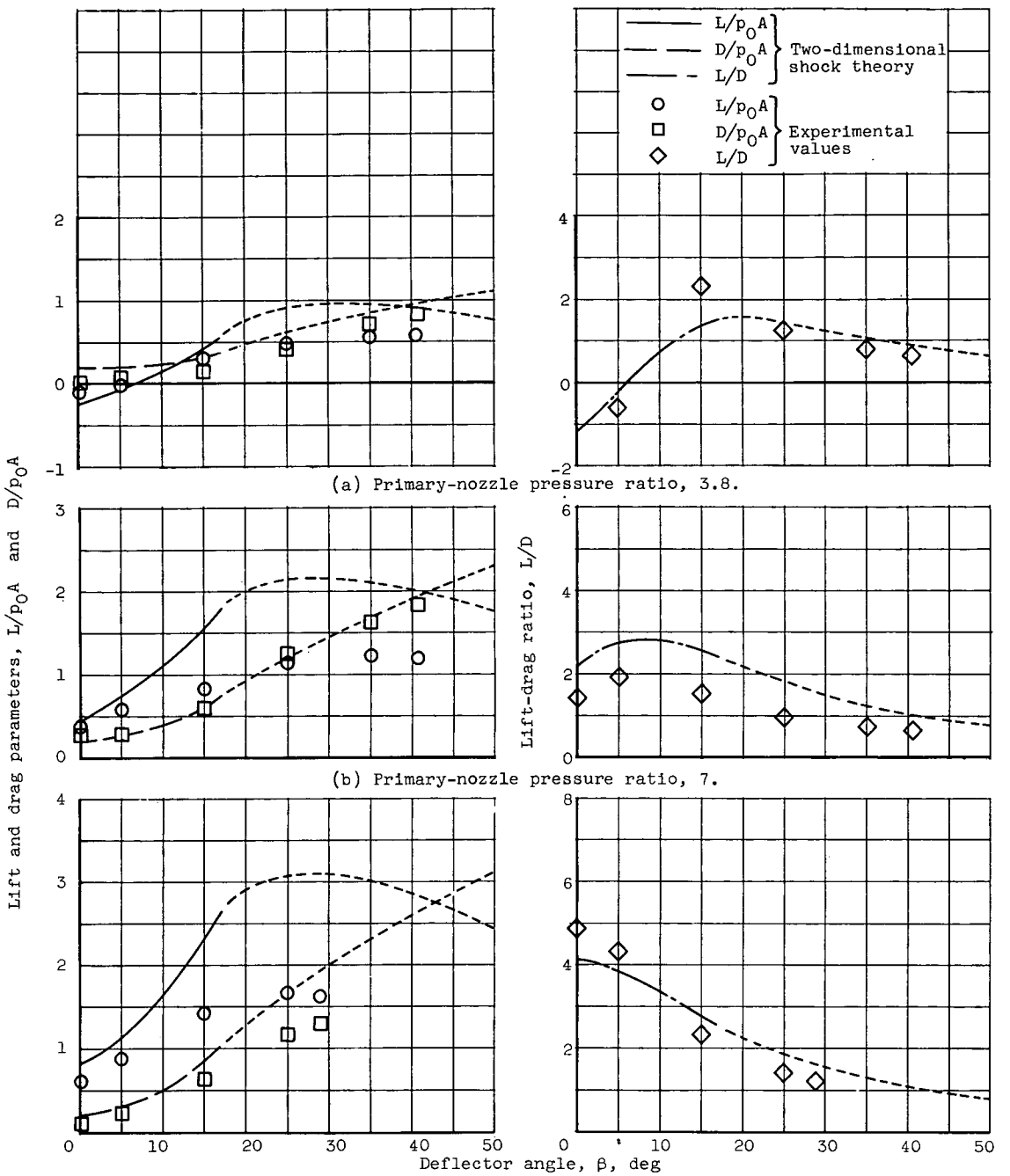

(a) Primary-nozzle pressure ratio, 3.8.

(b) Primary-nozzle pressure ratio, 7.

(c) Primary-nozzle pressure ratio, 9.

Figure 10. - Comparison of experimental data with two-dimensional shock theory. Configuration III; secondary-to-primary weight-flow ratio, zero.